ISSN 0031-918X, The Physics of Metals and Metallography, 2015, Vol. 116, No. 6, pp. 615–625. © Pleiades Publishing, Ltd., 2015.
Original Russian Text © N.N. Popov, T.I. Sysoeva, E.V. Shchedrina, D.V. Presnyakov, E.N. Grishin, 2015, published in Fizika Metallov i Metallovedenie, 2015, Vol. 116, No. 6, pp. 652–662.

STRENGTH AND PLASTICITY

Effects of the Regimes of Heat Treatment and of the Magnitude and Temperature of the Inducing Deformation on the Characteristics of the Shape-Memory Effect in the 43Ti–46Ni–9Nb–2Zr Alloy

N. N. Popov, T. I. Sysoeva, E. V. Shchedrina, D. V. Presnyakov, and E. N. Grishin

Russian Federal Nuclear Center, All-Russia Research Institute of Experimental Physics, pr. Mira 37, Sarov, Nizhni-Novgorod oblast, 607188 Russia

e-mail: popov@astra.vniief.ru

Received September 2, 2014; in final form, December 24, 2014

Abstract—The influence of the types and regimes of heat treatment, as well as of the temperature and magnitude of the shape-memory-inducing deformation on the structural changes, martensitic transformations, parameters of the crystal lattice and substructure, and the mechanical and thermomechanical characteristics have been studied in the new shape-memory alloy of composition 43Ti–46Ni–9Nb–2Zr (at %). The conditions of the appearance and realization of the shape-memory effect have been determined. The relationship between the structural features and the values of the thermomechanical characteristics of the alloy has been revealed. The regimes of the heat treatment and of the deformation that induces the shape-memory effect, which provide in this alloy the obtaining of high thermomechanical characteristics, have been determined.

Keywords: Ti–Ni–Nb–Zr alloy, shape-memory effect, heat treatment, magnitude and temperature of deformation inducing the shape-memory effect, structure, martensitic transformations, phase composition, mechanical characteristics, thermomechanical characteristics

DOI: 10.1134/S0031918X15060071

1. INTRODUCTION

In our previous works, we performed a number of studies concerning the thermomechanical characteristics (TMCs) of the shape-memory alloys (SMAs) of the Ti–Ni–Fe and Ti–Ni–Nb systems with a purpose to further develop different technologies on their basis [1–4]. However, at present, it has become necessary to expand the range of SMAs to be investigated and opportunities for their practical application via the search for new compositions and new regimes of their treatment [5, 6]. This determined the purpose of this work, i.e., to analyze the structure and martensitic transformations of a new SMA of composition 43Ti–46Ni–9Nb–2Zr (at %) and to search for regimes of its heat treatment and temperature–heating-rate conditions necessary for inducing deformations, which would ensure that the required magnitudes of thermomechanical characteristics suitable for the specified exploitation conditions are obtained. The solution of these problems should ensure the wide introduction of new unique materials with the shape-memory effect (SME) into the industry, in particular into the vigorously developing branch of nuclear energy. Note that, earlier [5], we published some results of a comparative study of the above-mentioned alloy after pressing and an alloy of a similar composition in the as-cast state.

2. EXPERIMENTAL

The investigations were performed on an SMA of composition 43Ti–46Ni–9Nb–2Zr (at %) of batch no.16-08-p. The bars of this alloy were in the as-pressed state. Table 1 gives the chemical composition of the alloy according to the data of the supplier. The samples for the investigation were prepared by the electrospark method. The samples for X-ray diffrac-

Table 1. Chemical composition of the as-received alloy

Specified composition of the alloy		Alloy composition according to the supplier, at %			
at %	wt %	Ti	Ni	Nb	Zr
43Ti–46Ni–9Nb–2Zr	35.6Ti–46.7Ni–14.5Nb–3.2Zr	42.9	45.9	9.2	2.0

tion studies had a cylindrical shape with threaded heads (M4), a total length of 26 mm, the length and diameter of the gage part of 14 and 3 mm, respectively; along the entire gage part of the sample, two symmetrical flats were made, the distance between which was 2 mm. To eliminate the work-hardened surface layer that appears in the process of manufacturing the samples, deep chemical etching in an aqueous solution of acids was used ($1/3HNO_3 + 1/3HF + 1/3H_2O$). Samples for studying the mechanical and thermomechanical characteristics also had a cylindrical form with threaded heads (M4), an overall length of 26 mm, and a length and diameter of the gage part of 14 and 2 mm, respectively. In each experiment, three to five samples were used. The microstructural studies were performed on polished samples subjected to mechanochemical treatment using a solution of colloidal silica, as well as to etching by argon ions.

The heat treatment (HT) of samples was carried out by quenching or annealing under the following conditions:

(1) quenching from 800°C, holding for 0.5 h, cooling in water (regime HT no. 1);

(2) annealing at a temperature of 600°C for 1 h, furnace cooling (the HT 2 regime);

(3) annealing in a vacuum at a temperature of 850°C for 4 h, furnace cooling (the HT 3 regime).

The deformation of the samples to generate the subsequent SME was performed by tension as follows:

(1) with different total deformation ε_0 (6, 11, 15, 25%) at a constant temperature $T_d = (-60...-70)$°C and a strain rate (of inducing the deformation) used upon the generation of the SME $\dot{\varepsilon} \approx 1.2 \times 10^{-3}$ s^{-1};

(2) at different deformation temperatures T_d ((−60...−70)°C, (0...−5)°C, 24°C) at a constant total deformation $\varepsilon_0 = 11\%$ and a strain rate $\dot{\varepsilon} \approx 1.2 \times 10^{-3}$ s^{-1}.

The phase composition and the microstructure of the alloy samples in the initial state and after HT under different conditions were determined locally using a MIRA-2 LMU scanning field-emission electron microscope, by the electron-microprobe method. The phase composition, parameters of the crystal lattice and substructure, and the characteristics of the martensitic transformation of the samples of the alloy in the initial state, were determined by the methods of X-ray diffraction analysis after HT and before and after achieving SME using an 18-kW diffractometer in Cu $K\alpha$ radiation. To study the characteristics of the martensitic transformation, the diffractometer was equipped with a temperature chamber ensuring the change in the temperature of −200 to +100°C.

The mechanical and thermomechanical characteristics were determined on samples in the initial state, after HT by different regimes, and under conditions used to achieve the SME and the two-way shape-memory effect (TWSME) according to the previously developed experimental methodical base [7].

To determine the mechanical characteristics of the alloy using a UTS-100K testing machine at temperatures $T = (-55...-70)$°C, the samples were subjected to tensile tests at a strain rate of 1.2×10^{-3} s^{-1}. Based on the stress σ–strain ε tensile diagrams, the principal mechanical characteristics were determined, i.e., the phase yield stress σ_{ph}, the yield stress of the material with the SME σ_y^{SMM}, the ultimate yield strength σ_u, and the maximum deformation of the sample before rupture ε_0^{max}. The relative elongation δ_{rel} was determined based on the results of room-temperature measurements of the initial length of the gage part of the samples and the length of the gage part after the rupture.

When conducting studies of the thermomechanical characteristics of the alloy, the samples were first subjected to a tensile deformation to a chosen total degree of deformation $\varepsilon_0 = 11\%$ at a strain rate of $\dot{\varepsilon} \approx 1.2 \times 10^{-3}$ s^{-1} at a temperature $T = (-55...-70)$°C using the UTS-100K testing machine. Immediately after the deformation, the samples were placed at negative temperatures into a heating chamber of the device preliminarily cooled to the same temperature in order to analyze the thermomechanical characteristics of the materials with the SME and heated to the temperature $T \sim 110$°C, then cooled. Based on the results of these studies, diagrams of the shape recovery and shape change of the samples were constructed that corresponded to the manifestation of the SME and TWSME, respectively. Based on these diagrams, the temperatures of the start ($A_{s, SME}$) and finish $A_{f, SME}$ of the shape recovery in the free state upon the manifestation of the SME, and the temperatures of the start ($M_{s, TWSME}$) and finish ($M_{f, TWSME}$) of the shape change upon the manifestation of the TWSME in the free state during cooling after the manifestation of the SME were determined by the method of tangents. The tangents were drawn to regions of the most intensive change in the deformation as function of temperature. According to these diagrams, the values of the induced tensile deformation ε_t, the value of the thermally reversible deformation of the shape recovery ε_{SME} in the absence of an opposition during the manifestation of the SME, as well as the amount of reversible deformation upon the manifestation of the TWSME ε_{TWSME} in the range of the forward martensitic transformation were determined. The degree of the shape recovery η_{SME} upon the manifestation of the SME in the range of the reverse martensitic transformation was determined as the ratio $\varepsilon_{SME}/\varepsilon_t$, and the degree of the manifestation of the TWSME η_{TWSME} in the range of the forward martensitic transformation was determined as the ratio $\varepsilon_{TWSME}/\varepsilon_t$.

Table 2. Elemental and phase composition of the 43Ti–46Ni–9Nb–2Zr alloy (at %) after various regimes of heat treatment

Regions of different atomic contrast	Atomic concentration, %	Phases	Atomic ratio Ni/Ti
Initial state			
Gray	$Ti_{43.8}Ni_{48.4}Nb_{4.8}Zr_{2.9}$	TiNi, alloyed with Nb and Zr	1.10
Dark gray, with sizes to 25 μm	$Ti_{56.2}Ni_{33.4}Nb_{8.8}Zr_{1.6}$	Ti_2Ni, alloyed with Nb and Zr	–
White, with sizes to 15 μm	$Ti_{8.6}Ni_{5.8}Nb_{84.7}Zr_{0.9}$	Nb, alloyed with Ti, Ni, and Zr	–
Black, with sizes to 15 μm	$Ti_{59.4}Nb_{3.9}C_{35.9}Zr_{0.2}$	Carbide (Ti,Nb)C	–
After quenching according to the HT 1 regime			
Gray	$Ti_{43.7}Ni_{50}Nb_4Zr_{2.2}$	TiNi, alloyed with Nb and Zr	1.14
Dark gray, with sizes to 25 μm;	$Ti_{58.3}Ni_{32.3}Nb_{8.2}Zr_{1.2}$	Ti_2Ni, alloyed with Nb and Zr	–
White, with sizes to 15 μm	$Ti_7Ni_{4.4}Nb_{87.5}Zr_{1.1}$	Nb, alloyed with Ti, Ni, and Zr	–
Black, with sizes to 15 μm	$Ti_{62.1}Nb_4C_{33.1}Zr_{0.8}$	Carbide (Ti,Nb)C	–
After quenching according to the HT 2 regime			
Gray	$Ti_{44.5}Ni_{49.1}Nb_{4.0}Zr_{2.4}$	TiNi, alloyed with Nb and Zr	1.10
Dark gray, with sizes to 20 μm	$Ti_{57.1}Ni_{33.2}Nb_{8.4}Zr_{1.3}$	Ti_2Ni, alloyed with Nb and Zr	–
White, with sizes to 15 μm	$Ti_{16.6}Ni_{4.5}Nb_{77.4}Zr_{1.5}$	Nb, alloyed with Ti, Ni, and Zr	–
Black, with sizes of up to 10 μm	$Ti_{56.2}Nb_{3.8}C_{38.2}Zr_{0.7}$	Carbide (Ti,Nb)C	–
After quenching according to the HT 3 regime			
Gray	$Ti_{44.4}Ni_{48.9}Nb_{4.5}Zr_{2.1}$	TiNi, alloyed with Nb and Zr	1.10
Dark gray, with sizes to 25 μm	$Ti_{57.1}Ni_{33.1}Nb_{8.7}Zr_{1.1}$	Ti_2Ni, alloyed with Nb and Zr	–
White, with sizes to 20 μm	$Ti_{12.6}Ni_{8.5}Nb_{77.9}Zr_1$	Nb, alloyed with Ti, Ni, and Zr	–

3. RESULTS AND DISCUSSION

3.1. Structure, Martensitic Transformations, and Mechanical and Thermomechanical Properties of the Alloy in the Initial State and after Different Heat Treatments

3.1.1. Microstructural studies. The investigations of the distribution of elements in the structure of the samples of the 43Ti–46Ni–9Nb–2Zr alloy in the initial state and after different regimes of HT, which were carried out on the images obtained in the EBSD regime by the method of electron-microprobe analysis, have shown the presence of four regions that exhibit different atomic contrast (Table 2). The analysis of these regions made it possible to identify the following phases in the alloy investigated:

(1) TiNi alloyed with niobium and zirconium;

(2) Nb alloyed with titanium, nickel, and zirconium;

(3) Ti_2Ni alloyed with niobium and zirconium;

(4) carbide of titanium and niobium (Ti, Nb)C, which has not been revealed in the alloy after annealing by the HT 3 regime.

The basic phase of the alloy, TiNi, has an enhanced concentration of nickel (atomic ratio Ni/Ti >1.07) due to the withdrawal of titanium into the Nb-based solid solution, as well as due to the formation of a Ti-rich intermetallic compound Ti_2Ni and the carbide phase.

The SEM images of the microstructure (Fig. 1) clearly demonstrate the heterophase nature of the structure, which in the samples of alloy in the initial state and after different HTs is identical. The basic phase, which consists of gray elongated fine grains, is the intermetallic compound TiNi (structure type *B*2), in which the atoms of titanium and nickel are partly replaced by niobium (to 4.8 at % in the initial state; from 4 to 4.5 at % after different HTs) and by zirconium atoms (to 2.9 at % in the initial state; from 2.1 to 2.4 at % after different HTs). In the intergranular spaces, a eutectic of lamellar or skeleton-like morphology is observed, which consists of alternating layers of the intermetallic compound TiNii and of Nb-based solid solution. The grain boundaries are bordered by white Nb inclusions of a rounded or lamellar shape, in which the niobium atoms are partly replaced by titanium, nickel, and zirconium. The structure of the alloy also contains separate dark gray inclusions, which are located in the softer component of the structure, i.e., the eutectic, and are identified as Ti_2Ni with impurities of niobium and zirconium, and

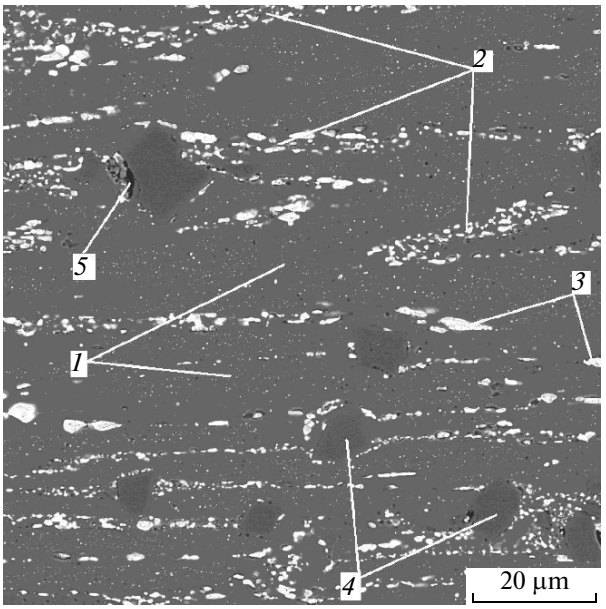

Fig. 1. Typical image of the microstructure of the 43Ti–46Ni–9Nb–2Zr (at %) alloy, obtained in the regime of the secondary electrons: (*1*) TiNi; (*2*) (Ti, Ni, Nb) eutectic; (*3*) Nb; (*4*) Ti_2Ni; (*5*) (Ti, Nb)C carbides.

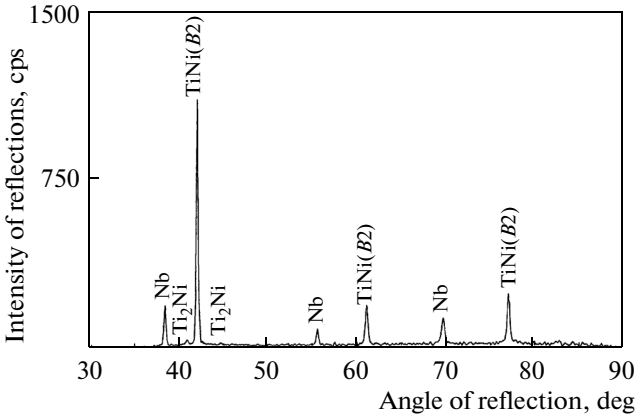

Fig. 2. Typical X-ray diffraction pattern of the 43Ti–46Ni–9Nb–2Zr (at %) alloy, which characterizes its phase composition in the initial state and after different regimes of HT.

black impregnations of carbides of titanium and niobium (Ti, Nb)C located predominantly inside the inclusions of Ti_2Ni. However, there are some distinctions in the microstructure of the samples; in the alloy after annealing according to the HT 3 regime, no carbides of titanium and niobium are present, while in the alloy that is in the initial state, martensitic regions are observed in the structure of separate regions of the titanium nickelide NiTi (*B*2) phase.

3.1.2. X-ray diffraction studies. The alloy investigated in the initial state and after HT under different conditions consists, according to X-ray diffraction data [8], of three phases (Fig. 2): titanium nickelide TiNi in the *B*2 state with an ordered bcc lattice, niobium Nb with a bcc lattice, and the Ti_2Ni phase with an fcc lattice. The content of particles of the Ti_2Ni phase determined by the method of semiquantitative XRD phase analysis is considerably greater in the samples after quenching according to the HT 1 regime (Table 3). This can hinder the growth of martensite crystals both inside the grains and at their boundaries and, as a consequence, lead to a decrease in the SME. The lattice parameter of the *B*2 TiNi phase in the samples of alloy after annealing according to the HT 3 regime is close to its known values for TiNi with allowance for its alloying with Nb and Zr. An increase in the lattice parameter of the *B*2 TiNi phase in the samples in the initial state, after quenching according to regime TO 1, and annealing according to HT 2 is explained by the influence of the residual stresses arising in this phase.

The dislocation substructure of the alloy calculated based on the data of the XRD analysis [8] in the initial (as-pressed) state is characterized by the strongly nonequilibrium grain boundaries, which contain dislocations with a density of 10^{11} cm^{-2}, with the size of blocks

Table 3. Percentages of phases and the lattice parameter of the TiNi phase (*B*2) in the samples of the 43Ti–46Ni–9Nb–2Zr alloy after different regimes of HT

Regime of HT	TiNi (*B*2), %	Nb, %	Ti_2Ni, %	Lattice parameter *a* (Å) of the TiNi (*B*2) phase
Initial state	59.1	30.0	10.9	3.0381
Quenching according to the HT 1 regime	56.7	21.9	21.4	3.0258
Quenching according to the HT 2 regime	62.6	27.9	9.5	3.0356
Quenching according to the HT 3 regime	76.4	16.1	7.5	3.0218

Table 4. Values of the basic mechanical properties of the samples of as-pressed alloy 43Ti–46Ni–9Nb–2Zr after HT according to different regimes

Regime of HT	σ_{ph}, MPa	σ_y^{SMA}, MPa	σ_u, MPa	ε_0^{max}, %	δ_{res}, %
Initial state	315	930	970	23.5	14
Quenching according to the HT 1 regime	250	890	910	30.5	23
Quenching according to the HT 2 regime	240	860	910	37.0	24
Quenching according to the HT 3 regime	280	870	930	40.5	25

of ~30 nm, and with the degree of microdeformation of the crystal lattice of about 10^{-3}. This leads to its additional strengthening and creating obstacles for the propagation of martensitic transformation. The subsequent heat treatment (quenching under the HT 1 regime and annealing according to the HT 2 regime) leads to the redistribution of dislocations and their partial annihilation, to an increase in the size of blocks, to their merging by one another, and to a reduction in the magnitudes of microdeformations in the crystal lattice. The annealing of the alloy according to the HT 3 regime leads to the complete elimination of the dislocation substructure. Obtaining this internal structure of the alloy as a result of HT serves as a prerequisite for a decrease in the level of the strength properties of the alloy in comparison with the initial state and, as a consequence, to an improvement of the shape-memory properties.

The study of the characteristics of the martensitic transformation of the 43Ti–46Ni–9Nb–2Zr alloy has demonstrated that no thermally activated martensite transformation occurred down to the temperature of cooling equal to 93 K (–180°C) either in the samples that are in the initial state or after HT according to different regimes. This is connected with the formation of a matrix enriched in nickel in the alloy, which leads to the shift of the range of the thermoactivated forward martensitic transformation into the region of subcryogenic temperatures.

3.1.3. Mechanical and thermomechanical characteristics. The mechanical characteristics of the alloy (Table 4) that have been determined from the tensile stress–strain diagrams (Fig. 3) depend strongly on the HT regime. It has been found that the use of heat treatment leads to an insignificant reduction in the strength properties in comparison with the initial state; the plastic properties in this case increase by a factor of 1.5–2. The best combination of plastic properties is characteristic of the alloy subjected to annealing according to the HT 3 regime, which is connected with the formation in this state of a structure, in which the crystal lattice is almost perfect and is not distorted; i.e., the amount of obstacles for dislocation slip in it is minimum, the lattice parameter is not changed, and the content of particles of the Ti_2Ni phase is minimum as well. As a consequence, this should lead to an increase in the maximum induced deformation, which determines the values of the reactive stresses [9], the reversible deformation, the degree of the shape recovery, and the temperature range of the shape recovery [10]. Moreover, the greater the amount of the induced deformation, the higher the level of the above characteristics should be.

The average values of the most important thermomechanical characteristics ($A_{s,\,SME}$, $A_{f,\,SME}$, ε_{SME}, η_{SME}, $M_{s,\,TWSME}$, $M_{f,\,TWSME}$, and $|A_{s,\,SME} - M_{f,\,TWSME}|$) determined from the diagrams given in Fig. 4 corresponding to the shape recovery and shape change in the sample upon heating and cooling have higher numerical readings after the annealing according to the HT 3 regime (Table 5).

Thus, the heat treatment (annealing) of the as-pressed 43Ti–46Ni–9Nb–2Zr alloy according to the HT 3 regime leads to a substantial change in the structure, i.e., to the dissolution of the carbide phase; to the removal of microdeformations of the crystal lattice; and to a decrease in the amount of defects, which impede the propagation of deformation and martensi-

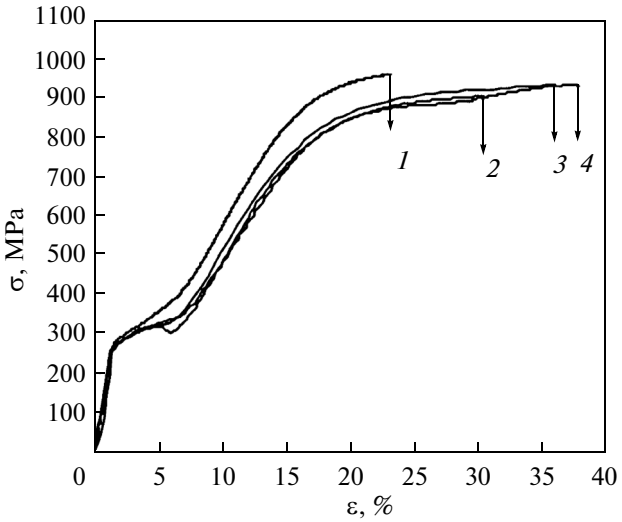

Fig. 3. Typical tensile stress–strain diagrams of the samples of the 43Ti–46Ni–9Nb–2Zr alloy after different regimes of HT: (*1*) in the initial state; (*2*) after quenching according to the HT 1 regime; (*3*) after annealing according to the HT 2 regime; and (*4*) after annealing according to the HT 3 regime.

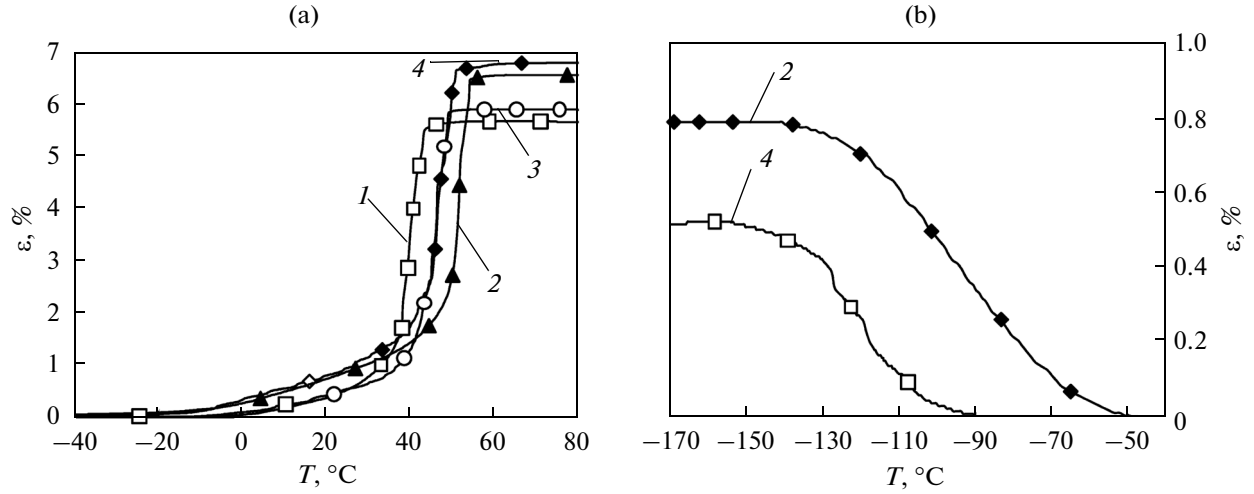

Fig. 4. Typical diagrams of (a) the shape recovery upon the manifestation of the SME and (b) of the shape change upon the manifestation of the TWSME for the samples of the 43Ti–46Ni–9Nb–2Zr alloy after different HT regimes: (*1*) initial state; (*2*) quenching according to the HT 1 regime; (*3*) annealing according to the HT 2 regime; and (*4*) annealing according to the HT 3 regime.

tic transformation. The formation of this structure leads to an improvement of the complex of mechanical properties, especially the plastic and shape-memory properties, which is a very important factor in controlling the technological properties of SMAs.

3.2. Study of Structural Features, Characteristics of the Martensitic Transformation, and Shape Recovery upon the Realization of the Shape-Memory Effect

3.2.1. X-ray diffraction studies. The reverse martensitic transformation in the 43Ti–46Ni–9Nb–2Zr alloy has been investigated by the X-ray diffraction method after annealing according to the HT 3 regime in the samples that manifest the SME upon heating after the induction of a preliminary tensile deformation under different conditions (by varying the amount of the induced deformation ε_0 at a constant temperature T_d of the deformation used to induce the SME; or by changing T_d at a fixed induced deformation ε_0).

Based on the data obtained for the characteristics of martensitic transformation (Table 6), it can be seen that, upon the deformation of the alloy samples to 6% by tension at (–60...–70)°C, martensite of the *B*19' type is formed. As the SME-inducing deformation increases from 6 to 15%, the amount of martensite increases. However, even in the case of large deformation (ε_0 = 15%), a fairly high portion of untransformed *B*2 austenite is retained (18%). The TiNi phase only passes completely from the austenitic *B*2 state into the martensitic state (*B*19') when the magnitude of the SME-inducing deformation reaches 25%. As a result of subsequent heating in the range of temperatures from –60°C to +100°C, the manifestation of the SME is observed and the TiNi phase undergoes reverse martensitic transformation, which, in samples

Table 5. Average values of the basis thermomechanical characteristics of the 43Ti–46Ni–9Nb–2Zr alloy after different regimes of heat treatment

Regime of HT	$A_{s,\,SME}$, °C	$A_{f,\,SME}$, °C	ε_{SME}, %	η_{SME}	$M_{s,\,TWSME}$, °C	$M_{f,\,TWSME}$, °C	ε_{TWSME}, %	η_{TWSME}	Hysteresis $\lvert A_{s,\,SME} - M_{f,\,TWSME}\rvert$, K
Initial state	36	45	5.8	0.75	*	*	*	*	*
Quenching according to the HT 1 regime	45	52	6.6	0.84	–73	–124	0.6	0.08	169
Quenching according to the HT 2 regime	42	50	5.9	0.72	*	*	*	*	*
Quenching according to the HT 3 regime	47	58	6.9	0.87	–100	–146	0.4	0.06	193

* The values have not been determined because of the absence of the manifestation of the TWSME.

Table 6. Schemes and the temperatures of the start and finish of the reverse martensitic transformation (MT) in the samples of the 43Ti–46Ni–9Nb–2Zr (at %) alloy that manifest the SME after induction of deformation under different conditions

Conditions used upon the induction of deformation	Scheme of MT with the indication of the percentage of *B*2 austenite and *B*19' martensite	Temperatures of the start and finish of the reverse MT upon the manifestation of the SME, °C		Width of the range $\lvert A'_{s,SME} - A'_{f,SME}\rvert$, K
		$A'_{s,SME}$	$A'_{f,SME}$	
$T_d = -60...-70$°C, $\dot{\varepsilon} \approx 1.2 \times 10^{-3}$ s^{-1}				
$\varepsilon_0 = 6\%$	62% *B*19' + 38% *B*2 → 100% *B*2	−15	15	30
$\varepsilon_0 = 11\%$	80% *B*19' + 20% *B*2 → 100% *B*2	25	40	15
$\varepsilon_0 = 15\%$	82% *B*19'+18% *B*2 → 100% *B*2	40	60	20
$\varepsilon_0 = 25\%$	100% *B*19' → 31% *B*2 + 69% *B*19'	60	>100	>40
$\varepsilon_0 = 11\%$, $\dot{\varepsilon} \approx 1.2 \times 10^{-3}$ s^{-1}				
$T_d = -60...-70$°C	80% *B*19' + 20% *B*2 → 100% *B*2	25	40	15
$T_d = 0...-5$°C	73% *B*19' + 27% *B*2 → 100% *B*2	30	50	20
$T_d = 24$°C	27% *B*19' + 73% *B*2 → 20% *B*19' + 80% *B*2	50	>100	>50

deformed to 6, 11, and 15%, occurs completely and is developed according to the scheme (*B*19' + *B*2) → *B*2. In the samples deformed to 25%, the transformation occurs not completely and is developed according to the scheme *B*19' → (*B*2 + *B*19'). Note that, in this case, heating was only conducted to a temperature of 100°C, which is connected with the limited capabilities of the equipment employed.

Upon the deformation of the alloy samples by tension at different temperatures (at a constant magnitude of the SME-inducing deformation equal to 11%), the *B*19' martensite is formed again. As the deformation temperature increases from (–60...–70)°C to 24°C, its amount decreases. In the case where the SME-inducing deformation is performed at a temperature of 24°C, the fraction of the arising martensite is small (27%). As a result of the subsequent heating from –60°C to 100°C, the TiNi phase undergoes, as a result of the manifestation of the SME, the reverse martensitic transformation, which in the samples deformed at temperatures of (–60...–70)°C and (0...–5)°C occurs completely and is developed according to the scheme (*B*19' + *B*2) → *B*2. In the samples deformed at a temperature of 24°C and heated to 100°C, the transformation occurs not completely and is developed according to the scheme *B*19' + *B*2 → *B*2 + *B*19'.

The results of the above investigation were used to determine the temperatures of the reverse martensitic transformation in the 43Ti–46Ni– 9Nb–2Zr alloy (the error of the measurements was ±5 K) caused by the manifestation of the SME due to tensile deformation performed under different conditions. It can be seen (Table 6) that as the deformation ε_0 that induces the SME increases from 6 to 25%, the values of the temperatures of the reverse martensitic transformation increase. This is connected with the presence of the *B*2 austenite in the phase composition of the samples before the onset of the reverse martensitic transformation and with its amount. According to [11], if both phases (both *B*2 austenite and *B*19' martensite) are present in the material at the moment of the change in the direction of the temperature variation and, thus, no nucleation of the new phase is required, the reverse martensitic transformation begins earlier than when the material is single-phase. In that case, the greater the amount of *B*2 austenite in the material, the earlier the transformation begins.

Based on the results of the investigation of the effect of temperature of the induction of deformation on the temperatures of the reverse martensitic transformation, two temperature intervals have been revealed. In the first range of the temperatures of the deformation induction, which lies in the range of (–60...–70)°C to (0...–5)°C, the temperatures of the reverse martensitic transformation upon the manifestation of the SME are almost independent of the temperature of the deformation T_d. In the second range of temperatures of the induction of deformation, which lies in the range of (0...–5)°C to 24°C, the temperature range of the reverse martensitic transformation $\lvert A'_{s,SME} - A'_{f,SME}\rvert$ expands and the temperatures of the reverse martensitic transformation upon the manifestation of the SME shift noticeably toward the higher temperatures. In this case, an especially strong shift is noted for the temperature $A'_{f,SME}$. This is due to the manifestation of the high-temperature SME, which is related to the stabilization of plastically deformed martensite ([12], pp. 329–332).

It was revealed that the lattice parameter of the *B*2 TiNi phase calculated after the manifestation of the

Table 7. Parameters of the substructure in the samples of the 43Ti–46Ni–9Nb–2Zr alloy after the manifestation of the SME upon the induction of tensile deformation under various conditions

Conditions of deformation		Degree of microdeformation of the lattice, 10^{-3}	Average size of blocks, nm	Density of dislocations, cm^{-2}	
				at the boundaries of blocks, 10^{11}	inside the blocks, 10^{11}
T_d = –60...–70°D, $\dot{\varepsilon} \approx 1.2 \times 10^{-3}$ s^{-1}	$\varepsilon_0 = 6\%$	1.4	25	5.1	0.2
	$\varepsilon_0 = 11\%$	2.1	20	7.3	0.4
	$\varepsilon_0 = 15\%$	3.2	15	11.2	1.0
	$\varepsilon_0 = 25\%$	3.3	15	14.2	1.0
$\varepsilon_0 = 11\%$, $\dot{\varepsilon} \approx 1.2 \times 10^{-3}$ s^{-1}	T_d = –60 ...–70°C	2.1	20	7.3	0.4
	T_d = 0 ...–5°C	1.9	20	8.6	0.3
	T_d = 24°C	2.9	15	12.7	1.2

Table 8. Average values of the thermomechanical characteristics of the 43Ti–46Ni–9Nb–2Zr alloy upon the manifestation of the SME after the induction of deformation under various conditions

Thermomechanical characteristics	Conditions of deformation						
	T_d = –60...–70°C, $\dot{\varepsilon} \approx 1.2 \times 10^{-3}$ s^{-1}				$\varepsilon_0 = 11\%$, $\dot{\varepsilon} \approx 1.2 \times 10^{-3}$ s^{-1}		
	$\varepsilon_0 = 6\%$	$\varepsilon_0 = 11\%$	$\varepsilon_0 = 15\%$	$\varepsilon_0 = 25\%$	T_d = –60...–70°C	T_d = 0...–5°C	T_d = 24°C
ε_t, %	4.3	8.0	11	18.4	8.0	6.8	6.0
$A_{s,\,SME}$, °C	8	47	50	72	47	32	51
$A_{f,\,SME}$, °C	25	58	64	104	58	51	97
ε_{SME}, %	3.0	6.9	7.7	7.3	6.9	4.5	0.6
η_{SME}	0.70	0.87	0.70	0.40	0.87	0.65	0.10
$\lvert A_{s,\,SME} - A_{f,\,SME}\rvert$, K	17	11	14	32	11	19	46

SME in the alloy samples has a higher value when the deformation ε_0 equal to 25% is induced in the alloy (at T_d = (–60...–70)°C, $\dot{\varepsilon} \approx 1.2 \times 10^{-3}$ s^{-1}) and when the deformation is induced at a temperature T_d = 24°C (at $\varepsilon_0 = 11\%$, $\dot{\varepsilon} \approx 1.2 \times 10^{-3}$ s^{-1}) than under other conditions of inducing deformation. This is because, under the above-mentioned deformation conditions, the TiNi phase exists in an intermediate two-phase state, i.e., the crystal lattice of the *B*19' phase is matched with the crystal lattice of the *B*2 phase and the atoms at the interphase boundary obey the crystalline order characteristic of both phases. The occurrence of good matching between the two lattices requires a certain elastic deformation in the place of joining, which generates an elastic field of coherent stresses. The appearance of stresses leads to a change in the lattice parameter.

The dislocation substructure of the alloy, which was formed after the manifestation of the SME in the alloy as a result of the induction of a preliminary tensile deformation in the range of ε_0 of 6–11% and in the range of the T_d temperatures from (–60...–70)°C to (0...–5)°C, is characterized by the minimum amount of dislocation-type structure defects. Correspondingly, the alloy contains a smaller amount of obstacles for the propagation of the martensitic transformation (Table 7).

3.2.2. Studies of thermomechanical characteristics (TMCs). The effects of the magnitude and temperature of deformation on the TMCs were investigated on the samples of the 43Ti–46Ni–9Nb–2Zr alloy subjected to annealing according to the HT 3 regime using the shape-recovery diagrams (Fig. 5) based on the manifestation of the SME after the induction of tensile deformation under different conditions. Table 8 contains the average values of the thermomechanical characteristics obtained in experiments and as a result of their statistical treatment taking into account the following instrumental errors: for the characteristic temperatures and for the hysteresis of the transformation, ±1 K; for the values of ε_{tens} and ε_{SME}, ±0.1%; and, for η_{SME}, ±0.01.

The statistical processing and the correlation analysis of the results of experiments [13, 14] have revealed a significant effect of the magnitude and temperature of the induction of deformation on each thermomechanical characteristic of the 43Ti–46Ni–9Nb–2Zr alloy. Thus, when the magnitude of the induced pre-

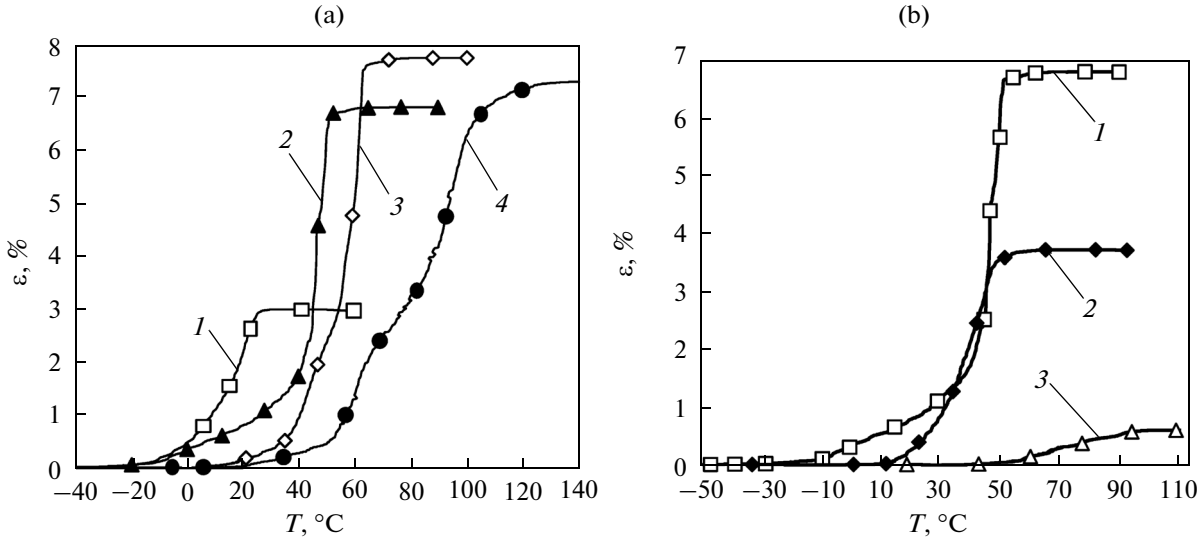

Fig. 5. Diagrams of shape recovery of the samples of the 43Ti–46Ni–9Nb–2Zr alloy obtained after the induction of the deformation: (a) at different values of the total deformation ε_0 ((*1*) $\varepsilon_0 = 6\%$, (*2*) 11%, (*3*) 15%, (*4*) 25%) and at constant $T_d = (-60...-70)°C$ and $\dot{\varepsilon} \approx 1.2 \times 10^{-3}$ s^{-1}; and (b) at different temperatures of deformation T_d ((*1*) $T_d = (-60...-70)°C$; (*2*) (0...–5)°C, (*3*) 24°C) and at constant $\varepsilon_0 = 11\%$ and $\dot{\varepsilon} \approx 1.2 \times 10^{-3}$ s^{-1}.

liminary tensile deformation increased from 6 to 25%, a linear increase in the values of ε_t, $A_{s,\,SME}$, and $A_{f,\,SME}$ was revealed, and a parabolic variation (first an increase, then a decrease) in the values of the parameters ε_{SME} and η_{SME} was observed. With an increase in the temperature of the induction of the preliminary tensile deformation in the range of (–60...–70)°C to 24°C, a linear increase was revealed in the values of the parameters $A_{f,\,SME}$ and $|A_{s,\,SME} - A_{f,\,SME}|$, a decrease in the values of the parameters ε_t, ε_{SME}, and η_{SME}, and parabolic variations (first a decrease, then an increase) in the parameter $A_{s,\,SME}$.

The obtained dependences of the values of the thermomechanical characteristics of the alloy on the values and temperatures of the induction of deformation are closely related to the structure, i.e., to the parameters of the substructure, the state of the basic phase before the manifestation of the SME, and the amount of this phase. Thus, the induction of the tensile deformation was carried out at a temperature of (–60...–70)°C. This temperature is located above the M_s temperature of the alloy. The deformation at this temperature leads to the obtaining of a two-phase state in the structure of the basic TiNi phase (which consists of *B*19' martensite and retained *B*2 austenite), which is achieved by two mechanisms, i.e., the nucleation of new martensite crystals and the reorientation of the existing martensite crystals under the effect of an external load. With an increase in the degree of deformation, the content of the retained *B*2 austenite decreases and the content of the *B*19' martensite increases, the mechanism of deformation changes, and there occurs only a reorientation of martensite crystals. The difference in the state of the basic TiNi phase before the manifestation of the SME leads to different values of the temperatures of the reverse martensite transformation. In regions where the basic TiNi phase is in the two-phase state (*B*19' martensite and the retained *B*2 austenite), no nucleation of crystals of the new phase (*B*2 austenite) is required; therefore, the reverse martensitic transformation begins earlier than in regions where the TiNi phase is in the single-phase state (*B*19'), and where the nucleation of the crystals of the new phase *B*2 is required (Table 6).

As follows from Table 8, the magnitude of the induced deformation after the removal of the load is somewhat less than that in the loaded state (i.e., $\varepsilon_t < \varepsilon_0$), and this difference increases with increasing deforming stress. The partial recovery of deformation upon the unloading is caused by the reversible displacement of intercrystallite and twin boundaries in the unloading–loading cycle, probably as a result of a change in the thermodynamic conditions of the thermoelastic equilibrium in the unstressed and stressed states. When the samples of the alloy are heated after deformation to the $A_{f,\,SME}$ temperature, the alloy manifests an SME; the degree of shape recovery η_{SME} in this case increases with increasing degree of deformation ε_0 to a certain value ε_{cr} (according to Table 8, to 15%), then decreases. The obtained regularity agrees well with the data given in [15]. The reduction in the degree of shape recovery η_{SME} upon deformation higher than 15% is connected with the accumulation of the irreversible carriers of deformation, first of all, dislocations. As follows from Table 7, upon the induction of preliminary tensile deformation of 6–11%, the formation of a

substructure occurs in the alloy, which is characterized by the presence of low-angle and nonequilibrium grain boundaries, which contain dislocations with a density on the order of 10^{11} cm^{-2}, and by the presence of microdistortions of crystal lattice on the level of 10^{-3} with blocks of 20–25 nm in size. The formation of this structure serves as a prerequisite for an increase in the dislocation yield stress and in the difference between it and the phase yield stress; however, in this case, the structure does not contain a high dislocation density inside the blocks. The obstacles for the reverse motion of the carriers of reversible deformation within the grain are minimum, which ensures a maximally complete realization of the shape recovery η_{SME} (0.70–0.87). The induction of the preliminary tensile deformation of 15–25% leads to an increase in the density of both free dislocations and grain-boundary dislocations by an order of magnitude (to 10^{12} cm^{-2}). The formation of this dislocation substructure creates obstacles for the reverse motion of carriers of reversible deformation, i.e., for the restoration of the shape (η_{SME} decreases to 0.40).

Based on the results of the investigation of the effect of the deformation temperature on the TMCs, two temperature intervals (Table 8) have been revealed. In the first range of the deformation temperatures, which lies in the range of (–60...–70)°C to (0...–5)°C, the values of the SME decrease gradually, but are still retained at a fairly high level. In the second range of the deformation temperatures, which lies in the range of (0...–5)°C to 24°C, the values of the SME fall sharply. This change in the TMCs is connected with the amount of the martensitic phase *B*19' and with the dislocation density, which could be obtained upon the induction of deformation at a specific temperature. In this case, it was revealed that the less the amount of the *B*19' phase and the greater the dislocation density obtained upon deformation, the worse the TMCs. Thus, the induction of deformation at temperatures of (–60...–70)°C and at (0...–5)°C makes it possible to obtain in the alloy the amounts of the martensitic phase *B*19' approximately equal to 80 and 73%, respectively, the dislocation density on the order of 10^{11} cm^{-2}, and a high complex of shape-memory properties, ε_{SME} = 4.5–6.9% and η_{SME} = 0.65–0.87. Upon the induction of deformation at a temperature of 24°C, only about 27% *B*19' martensite can be obtained in the alloy; in this case, the alloy is characterized by a high dislocation density (on the order of 10^{12} cm^{-2}) and a bad complex of SME properties (ε_{SME} = 0.6%; η_{SME} = 0.10).

4. CONCLUSIONS

(1) The structure, martensitic transformations, and mechanical and thermomechanical characteristics have been investigated for a new shape-memory alloy of composition 43Ti–46Ni–9Nb–2Zr (at %), for which no results of comprehensive studies are present in the literature. The conditions for the appearance and realization of the SME have been determined. The relationship between the structural features and the values of the thermomechanical characteristics of the alloy has been established.

(2) It has been revealed that the annealing of the as-pressed 43Ti–46Ni–9Nb–2Zr alloy in a vacuum at a temperature of 850°C for 4 h and the subsequent furnace cooling lead to a substantial change in the alloy structure, i.e., to the dissolution of the carbide phase and the removal of microdeformations in the crystal lattice, as well as a decrease in the amount of defects that can impede the propagation of deformation and of the martensitic transformation. The formation of this structure leads to an improvement of the complex of the mechanical properties, especially plastic, and of SME properties, which is a very important factor in controlling the technological properties of shape-memory alloys.

(3) It has been shown that the induction of deformation in the samples of the alloy in the range of 11–15% at temperatures in the range of (–60...–70)°C to (0...–5)°C at the strain rate of 1.2×10^{-3} s^{-1} makes it possible to obtain a maximum amount of the martensitic *B*19' phase in the alloy before the manifestation of the SME and a specific substructure with a minimum density of defects, such as dislocations. As a result of the formation of this structure, a high complex of the SME properties is obtained in this alloy (ε_{SME} = 6.9–7.7%; η_{SME} = 0.70–0.87), which can make it possible to use it in different devices, in particular in nuclear energy.

REFERENCES

1. N. N. Popov, *Development of Adanced Technologies Based on Shape-Memory Materials* (Russian Federal Nuclear Center, VNIIEF, Sarov, 2008) [in Russian].
2. N. N. Popov, S. D. Prokoshkin, M. Yu. Sidorkin, T. I. Sysoeva, D. V. Borovkov, A. A. Aushev, I. V. Kostylev, and A. E. Gusarov, "Effect of thermomechanical treatment on the structure and functional properties of a 45Ti–45Ni–10Nb alloy," Russ. Metall. (Metally), no. 1, 59–64 (2007).
3. N. N. Popov, T. I. Sysoeva, S. D. Prokoshkin, V. F. Lar'kin, and I. I. Vedernikova, "Mechanical properties and reactive stresses of Ti–Ni–Nb shape memory alloys," Russ. Metall. (Metally), No. 4, 310–316 (2007).
4. N. N. Popov, V. F. Lar'kin, D. V. Presnyakov, A. A. Aushev, T. I. Sysoeva, A. A. Kostyleva, and E. B. Suvorova, "Investigation of thermomechanical characteristics of shape-memory alloys of the Ti–Ni–Nb system and of the effect of heat treatment on them," Phys. Met. Metallogr., **114**, 348–357 (2013).
5. N. N. Popov, V. F. Lar'kin, T. I. Sysoeva, A. A. Aushev, and D. V. Presnyakov, "The study of structural peculiarities of thermomechanical and mechanical characteristics of new alloys of the Ti–Ni–Nb–Zr system with shape memory for the determination of possibility of

their application in technology of thermomechanical joining of pipelines," *Proc. Int. Sci.-Tech. Conf. "Innovation Projects and Technologies of Nuclear Energetics"* (OAO NIKIET, Moscow, 2012).

6. V. Ya. Abramov, N. M. Aleksandrova, D. V. Borovkov, S. Yu. Makushev, N. A. Polyakova, N. N. Popov, S. D. Prokoshkin, and I. Yu. Khmelevskaya, "Realization of reversible deformation, generation and relaxation of reactive stress in Ti–Ni–Nb(–Zr) alloys with a broad martensitic hysteresis," Materialovedenie, No. 7, 5–11 (2007).
7. N. N. Popov, "Experimental and methodical base for study of thermomechanical properties of shape-memory materials ," Zavod. Labor.: Diagn. Mater. **72**, 34–39 (2006).
8. N. N. Popov, A. I. Korshunov, A. A. Aushev, M. Yu. Sidorkin, T. I. Sysoeva, I. V. Kostylev, A. E. Gusarov, and V. V. Stolyarov, "Effect of nanostructurizing and rate of inducing deformation on the structural and thermomechanical characteristics of a titanium nickelide-based alloy," Phys. Met. Metallogr., **102**, 432–438 (2006).
9. N. N. Zakharova, S. L. Kuz'min, and V. A. Likhachev, "Large reversible deformations and plasticity of transformation in TiNiCu compositions," Metallofizika **3**, 84–88 (1981).
10. V. A. Likhachev and S. R. Shimanskii, *Effect of the Composition of a TiNiNb Alloy on Its Properties and Efficiency* (available from VINITI, Moscow, 1984, no. 7865-84).
11. V. E. Gyunter, V. N. Khodorenko, Yu. F. Yasenchuk, T. L. Chekalkin, V. V. Ovcharenko, A. A. Klopotov, G. Ts. Dambaev, P. G. Sysolyatin, N. G. Fomichev, V. N. Olesova, M. Z. Mirgazizov, A. V. Proskurin, R. V. Zigan'shin, V. K. Polenechkin, A. N. Matyunin, M. Yu. Fatyushin, N. A. Molchanov, and A. N. Monogenov, *Titanium Nickelide. Medical Material of New Generation* (Izd-vo MITs, Tomsk, 2006) [in Russian].
12. V. Brailovski, S. Prokoshkin, P. Terriault, and F. Trochu, *Shape Memory Alloys: Fundamentals, Modeling and Applications* (ETS, Montreal, 2003).
13. A. P. Kulaichev A.P. *Universal Program Statistical Package STADIA (version 7.0)* (Informatika i Komp'yutery, Moscow, 2007) [in Russian].
14. A. P. Kulaichev, *Methods and Tools of Complex Data Analysis* (Forum: Infra-M, Moscow, 2006) [in Russian].
15. *Materials with Shape-Memory Effect*, Ed. by V. A. Likhachev (NIIKh SPbGU, St. Petersburg, 1998), Vol. 4 [in Russian].

Translated by S. Gorin